

# Synthesis and Characterization of Monodisperse Uniformly Shaped Respirable Aerosols

**Catherine A. Fromen**

Dept. of Chemical and Biomolecular Engineering, North Carolina State University, Raleigh, NC 27695

**Tammy W. Shen**

Eshelman School of Pharmacy, University of North Carolina at Chapel Hill, Chapel Hill, NC 27599

**Abigail E. Larus**

Dept. of Chemistry, University of North Carolina at Chapel Hill, Chapel Hill, NC 27599

**Peter Mack and Benjamin W. Maynor**

Liquidia Technologies, Inc, Durham, NC 27713

**J. Christopher Luft**

Lineberger Comprehensive Cancer Center, University of North Carolina at Chapel Hill, Chapel Hill, NC 27599

**Joseph M. DeSimone**

Dept. of Chemical and Biomolecular Engineering, North Carolina State University, Raleigh, NC 27695

Eshelman School of Pharmacy, Dept. of Chemistry, and Lineberger Comprehensive Cancer Center, University of North Carolina at Chapel Hill, Chapel Hill, NC 27599

Sloan-Kettering Institute for Cancer Research, Memorial Sloan-Kettering Cancer Center, 1275 York Ave, New York, NY 10065

DOI 10.1002/aic.14157

Published online June 25, 2013 in Wiley Online Library (wileyonlinelibrary.com)

*The top-down, micromolding technique, referred to as Particle Replication in Nonwetting Templates (PRINT<sup>®</sup>), affords a new opportunity for the generation of inhalation therapeutics. Powders were fabricated with predetermined particle size and shape; when dispersed with a collision jet nebulizer, these particles resulted in monodisperse aerosols with geometric standard deviations well below 1.2. Dynamic shape factors for this novel set of uniformly shaped particles were determined by correcting the drag of nonspherical particles in the ultra-Stokesian flow conditions of the aerodynamic particle sizer (APS). This convenient approach for shape factor determination agreed well with current literature approaches and allowed for the correction of APS results for particles with known volumes. Determined shape factor values of PRINT geometries were used to estimate the theoretical median aerodynamic diameters of individual aerosols, which were then compared to actual inhalation powders. © 2013 American Institute of Chemical Engineers AICHE J, 59: 3184-3194, 2013*

**Keywords:** aerosols, biomedical engineering, nanotechnology, particle technology, particle/count/measurements

## Introduction

Due to the drastic improvements in aerosol device and particle engineering technologies in the past decade, the delivery of pulmonary therapeutics from a dry powder has become an area of great interest. Dry powder devices offer many benefits including patient actuation, a capacity to deliver a wide range of therapeutics, and the avoidance of cold chain storage issues. Despite the encouraging prospects, inhalation powders currently have limited application due to the complexities of these systems. Inhalation powders are

typically multicomponent systems, which must be entrained and deagglomerated in a desired manner before flowing through complex airway geometries and depositing in a target area of the lung.<sup>1-4</sup> Unsurprisingly, performance of these powders can vary dramatically. A key cause of this variability stems from the limited understanding of the interplay between an individual particle and its dynamic environment. Few studies have been performed on powders of controlled particle geometry, or even drug-only powder formulations, to address these concerns. Current technologies used to generate powders for inhalation products typically involve bottom-up approaches such as spray drying or precipitation reactions; these approaches often have restricted flexibility in particle composition and size distribution.<sup>5,6</sup> The ability to engineer aerosols in a predetermined fashion with complete

Correspondence concerning this article should be addressed to J. M. DeSimone at desimone@unc.edu.

control over particle size, shape and composition, and, thus, aerosolization is lacking. Owing to fabrication difficulties in creating monodisperse particles, the creation of truly monodisperse aerosols for inhalation studies has only been achieved in limited cases.<sup>7,8</sup> A perfectly monodisperse aerosol would be comprised of a uniform population of identical, unaggregated particles, indicated by a geometric standard deviation (GSD) equal to 1. In practice, a GSD less than 1.22 is typically referred to as “monodisperse”.<sup>7–9</sup> The formation of monodisperse aerosols would lend insight into the many physical principles at play in inhalation powders, contributing to optimized performance and improved dose uniformity to the patient.

Of the many physical parameters at play in aerosol formulations, particle shape is known to be a critical factor of behavior, and yet, in practice, little has been experimentally investigated.<sup>5</sup> Nonspherical aerosols in flow are not easily described through analytic approaches and are typically characterized in the aerosol community by a dynamic shape factor ( $\chi$ ).<sup>9–11</sup> A shape factor is used to correct for any differences in particle motion resulting from a nonspherical geometry by relating the drag of the nonspherical particle to that of an equivalent volume sphere. This term is defined in a Stokes’ flow regime (where Reynolds number  $Re$ , is less than one), which is relevant to low-velocity airstreams encountered in the bronchoalveolar regions of the lung (branched generations 18 and higher).<sup>9,12</sup> A particle’s dynamic shape factor contributes to the definition of the particle’s aerodynamic diameter ( $D_{AE}$ ), the main predictor of lung deposition.<sup>5, 9,11</sup> Determining an appropriate  $\chi$  for irregularly shaped particles is not trivial and much work has gone into the determination of the  $\chi$  for specific geometries. A limited data set for  $\chi$  determined through macroscale models exists for simple geometric shapes and dusts, with empirical relations extending for symmetric objects, such as spheroids, oblates and prisms.<sup>9,13–17</sup> A broader approach to define  $\chi$  using projected area and surface area has been established which successfully predicts the current set of literature values.<sup>18</sup> Finally, shape factors have been indirectly measured through use of elutriation devices, or simultaneous measurements of both an aerodynamic particle sizer (APS) spectrometer and an Andersen cascade impactor (ACI).<sup>18,19</sup> However, a rapid method for experimentally determining shape factor is lacking.

It is important to emphasize that  $\chi$  is an approximation; any contribution to drag experienced by the particle will be lumped into this single correction term. As with any such correction factor, it is worth briefly addressing the strengths and weaknesses of this approach. The dynamic shape factor approximation is commonly used in the aerosol literature to reduce the otherwise complicated physical characteristics of a nonspherical particle to a much simpler spherical one. By discussing particles in terms of equivalent spheres, as illustrated in Figure 1, established properties of spherical aerosols can be rapidly translated to nonspherical ones. In terms of respiratory drug delivery, this enables predictions of particle deposition in different lung regions based solely on  $D_{AE}$ . In most situations of aerosol work, this approximation is extremely useful; long length and time scales in most flow applications result in a reasonable simplification to spherical properties. However, in cases where these length or time scales are reduced, use of  $\chi$  will not appropriately account for individual particle dynamics. The precise drag of a nonspherical particle depends on the geometry and the orientation of the

particle, which are not differentiated using a shape factor simplification.<sup>13</sup> Additionally, the influence of torque and lift, known to contribute to aerodynamics of nonspherical particles, are not taken into account.<sup>10</sup> While understanding of individual particle dynamics based on geometry will be increasingly influential to the literature,  $\chi$  characterization will continue to be the standard in the aerosol community as it is an extremely useful simplification.

By quantifying  $\chi$  for nonspherical particles, the role of particle geometry can be investigated for entrainment, deagglomeration, flow and deposition in airways. For respiratory delivery, particle geometry is also known to influence mucociliary clearance, macrophage uptake and drug release kinetics.<sup>4,20–23</sup> Investigating particle behavior and shape effects in each of these areas could lead to novel strategies for the design of efficient inhaled drug delivery systems. As such, there is an unmet need to create monodisperse shaped particles to perform these studies. Knowledge gained on the behavior of precisely shaped particles as powders and aerosols could be used to optimize performance in the various stages of pulmonary drug delivery. PRINT, a top-down, roll-to-roll nano- and micromolding technique has been used to fabricate particles with unprecedented control over size, shape and composition; this platform has been applied to the creation of dry power formulations, with the application for inhaled drug delivery.<sup>22,24–26</sup> While previous work has shown that the PRINT micromolding technique is capable of fabricating monodisperse particles as dispersions in liquid, their quality as dry powder aerosols has yet to be explored in depth. The object of this work was to fabricate monodisperse particles relevant for dry powder therapeutics and explore the influence of particle shape on flow and dispersion. Enabled by these inherently monodisperse particles, we also explored a novel method for characterizing aerosol shape factors through APS measurements in attempt to further characterize aerosol behavior of nonspherical particles.

## Theory

### Shaped particles in Stokes’ flow

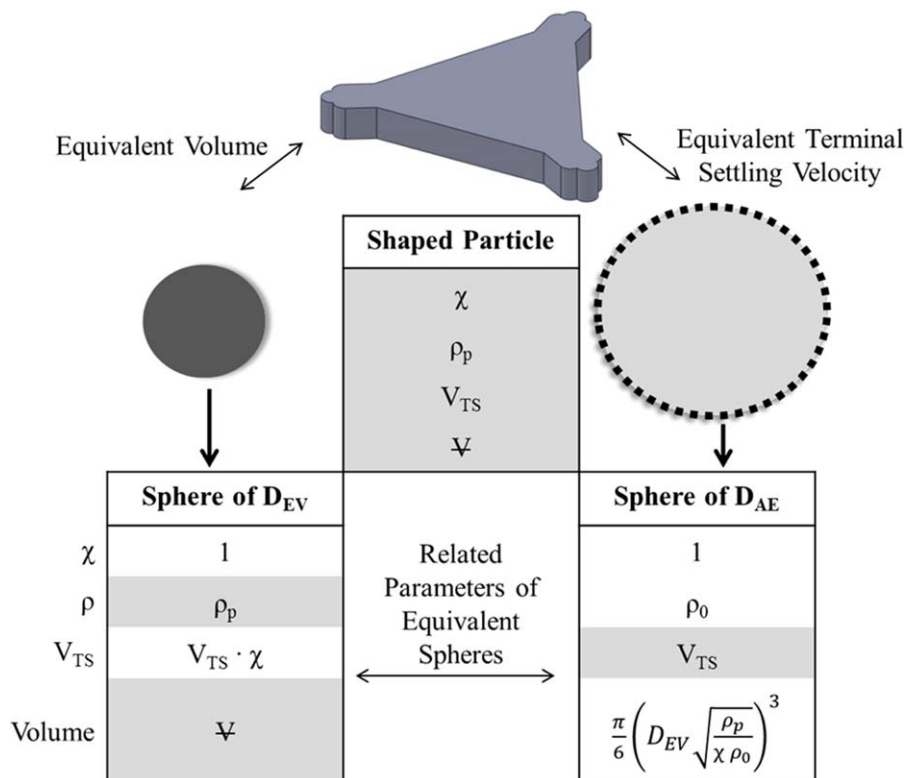
Aerosols of respirable size ( $D_{AE} \sim 1\text{--}5 \mu\text{m}$ ) that settle in air are typically considered to fall under the assumption of Stokes’ flow.<sup>9</sup> Under these conditions, an aerosol’s dynamic shape factor is implemented to correct the drag force on nonspherical particles from that of a sphere. In Stokes’ flow, the drag force of a nonspherical particle becomes

$$F_{D-\text{shaped}} = \chi \cdot F_{D-\text{sphere}} = \chi \cdot \frac{3\pi\mu D_{EV}V}{C_C} \quad (1)$$

where  $F_D$  is the drag force,  $\mu$  is the fluid viscosity,  $D_{EV}$  is the diameter of a sphere with a volume equivalent to the shaped particle,  $V$  is the particle velocity, and  $C_C$  is the Cunningham slip correction factor, defined as

$$C_C = 1 + \frac{2\lambda}{D_{EV}} \left[ 1.257 + 0.4 \left( -\frac{1.1D_{EV}}{2\lambda} \right) \right] \quad (2)$$

where  $\lambda$  is the mean free path of the fluid, typically air.<sup>9,11</sup> These expressions are valid for  $Re$  less than 1 and assumes a no slip boundary condition at the surface of the particle. As the particle size drops below  $10 \mu\text{m}$ , the no slip condition is no longer valid; the  $C_C$  term is needed to correct for slip in this regime and its contribution becomes increasingly significant as particle size decreases.<sup>9</sup> Eq. 2 is considered valid for



**Figure 1. Nonspherical particle and its equivalent spheres.**

Parameters shared between the equivalent sphere and the nonspherical particle are highlighted. [Color figure can be viewed in the online issue, which is available at [wileyonlinelibrary.com](http://wileyonlinelibrary.com)]

particle sizes 10  $\mu\text{m}$  and below and, as it is a function only of  $D_{EV}$ , it can be reasonably applied to correct slip for nonspherical particles.<sup>9,11</sup>

Dynamic shape factor is experimentally defined by measuring the terminal settling velocity ( $V_{TS}$ ) of a particle. Equating the Stokes' drag force in Eq. 1 with the gravitational force allows for the expression of  $V_{TS}$  for an aerosol

$$V_{TS} = \frac{\rho_p D_{EV}^2 g C_C}{18\mu\chi} \quad (3)$$

where  $\rho_p$  is the particle density,  $g$  is the acceleration due to gravity. Equation 3 is valid over all particle sizes, assuming Stokes' flow.<sup>9</sup> From Eq. 3, measurement of  $V_{TS}$  for a nonspherical particle in a situation of known fluid properties allows for the determination of the corresponding dynamic shape factor.<sup>27,28</sup> Importantly,  $\chi$  can be used to determine the particle's  $D_{AE}$  through the following relation

$$D_{AE} = D_{EV} \left( \frac{\rho_p C_C(D_{EV})}{\rho_0 \chi C_C(D_{AE})} \right)^{1/2} \quad (4)$$

where  $\rho_0$  is a standard particle density (1.0  $\text{g/cm}^3$ ).<sup>9</sup>

#### **Extension of dynamic shape factor in the non-Stokesian flow of an aerodynamic particle sizer (APS)**

The previous relation for particle drag can be applied only for  $Re$  less than one. However, the APS used to size aerosols in the following experiments operates at a flow rate which corresponds to a  $Re$  between 0.01 and 160.<sup>29</sup> Due to this operation outside Stokes' regime, corrections to the APS for errors measuring coincidence events, particle density and shape have been investigated in the literature.<sup>9,19,29–33</sup> As shown previously, the

APS technique is known to undersize nonspherical particles.<sup>9,19,32–34</sup> To account for this and correct APS measurements for nonspherical PRINT particles, an expression for shaped particles outside Stokes' flow must be considered.

As  $Re$  increases, the particle drag in Eq. 1 becomes dependent on flow conditions. In the non-Stokesian regime, an additional factor is included in the drag constant. For  $Re$  less than  $\sim 100$ , which is within the conditions of the APS for particles less than 10  $\mu\text{m}$ , there are a few commonly used ultra- or near-Stokesian correction terms.<sup>29</sup> In this work, the following expression was used to describe the particle drag

$$F_{D\text{-shaped}} = \chi \cdot \frac{3\pi\mu D_{EV}}{C_C} (U - V) (1 + 0.155 Re^{0.678}) \varphi^{-1/4} \quad (5)$$

where  $U$  is the fluid velocity.<sup>19</sup> The sphericity term  $\varphi$  is related to particle shape factor by

$$\varphi = \frac{2.188}{\chi} - 1.275 + 0.087\chi^3 \quad (6)$$

In the literature, the sphericity term in Eq. 6 has been validated for  $\chi$  ranging from 1 to 1.5. In this work,  $\varphi$  will be considered over all shape factors, as other ultra-Stokesian corrections assume empirical values that are equally untested at  $\chi$  greater than 1.5.

In tandem with the flow profile present in an APS spectrometer, these expressions can be used to correct for the aerodynamic effects of particles with known volume.<sup>33</sup>

## **Experimental**

### **Particle fabrication**

*Particle Fabrication using PRINT.* Particles were fabricated using the PRINT micromolding technique, described in

detail previously.<sup>25,26</sup> Highly crosslinked polymer networks were chosen as a model particle composition to explore the macroscale physical properties of shaped aerosols. PRINT molds (Liquidia Technologies) were filled by a lamination technique. A preparticle solution composed of 97 wt % 1,6-hexanediol diacrylate (HDODA), 2 wt % methacryloxyethyl thiocarbamoyl rhodamine B (PolySciences) and 1 wt % diphenyl(2,4,6-trimethylbenzoyl)phosphine oxide as a photoinitiator was cast onto a sheet of poly(ethylene terephthalate) (PET) and applied to the patterned PRINT molds. Open-faced, filled molds were photocured under ultraviolet light in a N<sub>2</sub>-purged, UV-LED oven for 30 s. Solid particles were then harvested onto a thin film of poly(vinyl alcohol) (PVA) coated on PET and collected by dissolving the film in water. Additional washes were performed to remove excess PVA. Finally, particles were lyophilized from *tert*-butanol to obtain dry powder samples. This process was repeated for each of the 14 geometries investigated in these studies. All chemicals and reagents were obtained from Sigma Aldrich unless noted.

**SEM Characterization.** Particle uniformity and morphology was confirmed using scanning electron microscopy (SEM). Samples were sputter-coated with 1–5 nm of Au/Pd (Cressington Scientific Instruments) and imaged (Hitachi model S-4700). SEM micrographs were used to measure feature sizes of each shape using ImageJ.<sup>35</sup> From these measurements, geometric properties, such as particle volume  $D_{EV}$ , and total surface area, were calculated.

**Bulk Density Measurements.** The density of the particle matrix was assumed to be equivalent to the density of a bulk sample of HDODA. Bulk samples were prepared by polymerizing 1 mL of preparticle solution on a glass slide in a N<sub>2</sub>-purged UV-LED oven for 5 min. Samples were then weighed in air and water using a density conversion kit for an analytical balance (Mettler Toledo). Bulk density was then calculated

$$\rho_p = \rho_{\text{Bulk}} = \frac{M_{\text{air}}}{M_{\text{water}}} (\rho_{\text{water}} + \rho_{\text{air}}) + \rho_{\text{air}} \quad (7)$$

where  $M_{\text{air}}$  is the mass of the bulk sample in air,  $M_{\text{water}}$  is the mass of the sample in water,  $\rho_{\text{water}}$  is the density of water, and  $\rho_{\text{air}}$  is the density of air.<sup>36</sup>

## Aerosol characterization

**Aerosol Characterization using APS.** Aerosol sizing was performed using an APS spectrometer (Model £ 3321, TSI, Inc.). An APS sizes aerosol particles by directing flow through a nozzle past two parallel lasers, where scattering events lead to measurements of a residence time; this residence time was calibrated to accurately size spherical aerosols of unit density. Particles were dispersed from methanol using a collision jet-nebulizer (CJN, MRE 1-jet, BGI, Inc.) which was connected to the APS through four feet of tubing which acted as a drying column. Due to the propensity for plastic tubing to charge aerosols through triboelectrification, glass tubing was chosen to minimize electrostatic charging of the aerosols and care was taken to ground the tubing.<sup>9</sup> A controlled leak was placed into the tubing to allow additional air into the column, ensuring conditions for the methanol to evaporate and resulting in methanol-free, monodisperse particles entering the APS. The APS sampled the nebulized aerosol for 5 min and readings of the number median aerodynamic diameter (NMAD) and GSD were recorded.

**Aerosol Characterization using an Andersen Cascade Impactor (ACI).** An Andersen cascade impactor (ACI, ThermoScientific) was used to size powder aerosol samples. Samples were dispersed by three different devices to evaluate the effectiveness in creating aerosols. A PennCentury insufflator device and a volume-calibrated hand pump (PennCentury, Inc.) were used to disperse dry powder samples, with typical fill weights of 2–5 mg. A Monodose inhaler device (Mod. 8, Plastiap SpA) was also used during ACI sizing, with 10 mg of dry powder samples loaded into hydroxypropyl methylcellulose (HPMC) capsules (Plastiap SpA). Finally, a CJN was employed as a control method for ensuring the creation of monodisperse aerosols.

ACI measurements were performed following standard protocol.<sup>37</sup> Before testing, collection plates were coated with poly(ethylene glycol) 300 and, following assembly, the flow rate was set and ambient conditions recorded. To avoid charging, the ACI was carefully grounded. The dispersion device was then attached to the ACI throat and tested at 28.3 L/min for 8 s. Deposited particles were collected from the device, throat, collection stages, and filter using a known volume of water. Polymer particles were analyzed through fluorescence spectrometry (SpectraMax M5 plate-reader) to obtain fluorescence intensities from the rhodamine B dye in the particle matrix. This corresponded directly to the relative mass deposited on each plate; from these, mass median aerodynamic diameters (MMADs) were calculated as the midpoint diameter ( $d_{50}$ ) from the cumulative fraction distribution. In a lognormal population, the geometric standard deviation (GSD) can be calculated from ratios of various diameters of the cumulative fraction distribution

$$GSD = \sigma_g = \frac{d_{84}}{d_{50}} = \frac{d_{50}}{d_{16}} = \left( \frac{d_{84}}{d_{16}} \right)^{1/2} \quad (8)$$

These expressions are equivalent for an ideal aerosol with a lognormal distribution, which is not true of aerosols with different distributions. As the aerosols studied here are not expected to be lognormally distributed, reported GSDs were consistently calculated using the first expression:  $\sigma_g = d_{84}/d_{50}$ .<sup>9</sup>

## Determination of Shape Factors

### Numerical APS model for shape factor calculation

As mentioned previously, the APS operates under non-Stokesian flow conditions. The correction for shaped particles, as derived in Eq. 5, is not taken into account during APS measurements and, as such, the APS incorrectly sizes nonspherical particles.<sup>9,14,24–26</sup> For a particle of both unknown size and unknown shape, it is difficult to correct for this underestimation. However, with a uniformly shaped particle of known dimensions, such as the particles made with PRINT, particle volume can be established. Measured APS results were corrected and the degree of underestimation from these results was used to determine particle shape factors. Following similar adjustments determined from previous work, we extended an appropriate model to account solely for the deviation of particle shape and were able to establish shape factors for PRINT geometries.

The drag experienced by a shaped particle was shown in Eq. 5. Applying Newton's second law, the following expression for particle velocity in the nozzle was established<sup>19,33</sup>



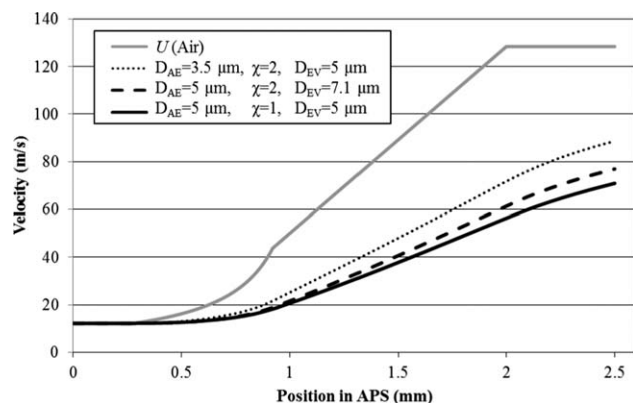
$$\frac{dV}{dx} = \frac{18\chi\mu}{\rho_p D_{EV}^2 C_C} \frac{(U-V)}{V} (1 + 0.155 Re^{0.678}) \varphi^{-1/4} \quad (9)$$

This again assumes a  $Re$  less than 100. Assuming inviscid, isothermal, compressible flow and using the geometry of the APS nozzle, an expression for the axial profile for air velocity through the nozzle  $U$ , was applied.<sup>33</sup> This background profile is shown in Figure 2. Equation 9 was solved numerically to generate a particle velocity profile through the APS nozzle as a function of physical parameters.<sup>38</sup> The calculated velocity within the APS nozzle for three different particle types are also shown in Figure 2: a sphere of unit density and two nonspherical particles, each with a  $\chi$  of 2 but with different volumes. This figure highlights the error inherent to the APS; not only does a particle of different  $\chi$  but equivalent  $D_{EV}$  have a markedly different velocity profile in the nozzle, but a particle of equivalent  $D_{AE}$  also experiences a different velocity profile due to the non-Stokesian flow regime. This deviation accounts for the underestimation attributed to the APS sizing of nonspherical particles.

In the numerical approach, two timing lasers were defined at position 2.2 and 2.323 mm based on the APS nozzle geometry. The residence time between the two lasers was determined by integrating the particle velocity over the laser positions.<sup>33</sup>

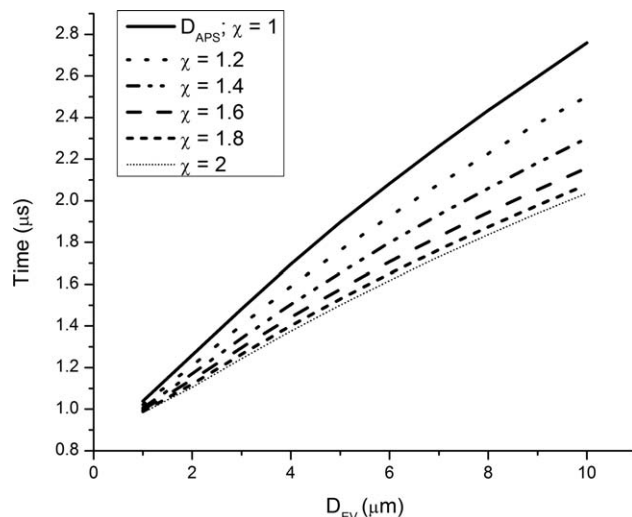
$$T = \int_{2.2}^{2.323} \frac{1}{V} dx \quad (10)$$

The residence time  $T$ , for spheres of unity density was then calculated to establish the base calibration used by the APS; these residence time measurements are used by the APS to define particle size. This calibration is shown by the solid curve ( $\chi = 1$ ) in Figure 3. However, varying the particle physical parameters, such as  $\chi$  or  $\rho$ , has a direct influence on APS residence time. Equation 9 can be used to predict  $T$  as a function of  $\chi$ ,  $D_{EV}$  and  $\rho$ . Figure 3 illustrates the residence time of nonspherical particles as a function of increasing  $\chi$  over a range of  $D_{EV}$ . Particles of a larger  $\chi$  will travel through the timing region at a higher velocity (as in Figure 2) and will obtain a smaller residence time (as in Figure 3). A few important points highlighting APS sizing



**Figure 2. Theoretical velocity profiles through the APS nozzle.**

The gray curve represents  $U$ , the background air profile. Particle velocities shown for a sphere (solid black) and particles with a shape factor equal to two with an equivalent volume (short dash) and equivalent aerodynamic diameter (long dash) to the spherical particle.



**Figure 3. Calculated APS residence times for particles of different sizes with varied shape factor.**

errors emerge from Figure 3. The deviation in residence time between a spherical and nonspherical particle becomes increasingly pronounced for larger particle volumes ( $D_{EV}$ ). Figure 3 also emphasizes that a given residence time can correspond to numerous particle geometries, contrary to the APS analytics. In a typical system of unknown particle size, shape and density, this oversight cannot be easily corrected. With particles of uniform size, shape and density, however, the only unknown is particle shape factor.

In tandem with experimental measurements, particle shape factors were determined by correcting APS measurements. From the values of residence time of unit density spheres, a calibration curve predicting  $D_{APS}$  was generated, as shown in Figure 3. Accordingly, for  $D_{APS}$  values measured experimentally from monodisperse aerosols, a corresponding residence time ( $T_{expAPS}$ ) was determined. Assuming a known  $D_{EV}$  from SEM measurements and known particle density from bulk sample measurements, shape factor was the remaining unknown in Eq. 9 and 10. Solving numerically and iterating over  $\chi$  values to fit calculated residence time to  $T_{expAPS}$ , shape factors ( $\chi_{APS}$ ) were determined for each geometry.<sup>38</sup>

**Sedimentation Tank for Shape Factor Determination.** Experimental determination of shape factor in a sedimentation tank ( $\chi_{sed}$ ) was performed following procedures similar to those in the literature.<sup>15,27,28</sup> A clear polycarbonate tank (diameter 20 cm height 30 cm) was filled with high-viscosity synthetic air compressor oil ISO grade 220, SAE grade 50 “Chemlube822” (UltraChem, Inc.) so that  $Re$  was maintained less than 0.1. Macroscale models of PRINT aerosols were created using a rapid prototyping method and were scaled two thousand times the original dimensions (volumes  $\sim 0.25$  cm<sup>3</sup>). Fluid viscosity was calibrated as a function of temperature throughout the experiment using polystyrene spheres (diameters ranging from 0.1 to 0.9 cm), which were timed over a drop of 15 cm.<sup>27</sup> Spheres and macroscale models were released  $\sim 5$  cm beneath surface of the fluid and in the center of the tank to neglect edge effects. Model parts were released from a controlled orientation and timed over a 15 cm drop. Each trial was replicated 10 times for each starting orientation, and then replicated over five copies of each model part. Initial release included a horizontal position (Exp-H) to maximize the surface area facing the bottom of

the tank and a vertical position (Exp-V) to minimize the surface area facing the bottom of the tank. Using Eq. 3,  $V_{TS}$  was determined by dividing the known fall distance over time. Assuming a  $C_C$  of one, shape factor ( $\chi_{sed}$ ) values were computed.

Shape Factor Determinations from Additional Literature Approaches. An additional approach existing in the literature for shape factor determination involves a relationship between the projected area and surface area.<sup>18</sup> This approach makes use of two additional equivalent spheres; for each nonspherical particle, a sphere of equivalent surface area and equivalent projected area is defined in addition to those shown in Figure 1. Empirical relationships have been established to relate these four equivalent spheres to calculate shape factor, which fit to previously determined shape factors in the literature. Calculations for shape factor ( $\chi_{PSA}$ ) of PRINT geometries were evaluated by assuming the maximum projected area of a given particle, the equivalent to orientation Exp-H in the settling tank experiment. Using SEM measurements of particle geometries, equivalent spheres were established and  $\chi_{PSA}$  calculated using the expressions derived by Leith.<sup>18</sup>

The final comparison of shape factor determination was performed by approximating each shape as an oblate ( $\chi_{Oblate}$ ).<sup>13</sup> Empirical expressions exist for the drag on oblate geometries; a common approach in the literature is to assume oblate dimensions which can encase nonspherical particles in order to apply these expressions. This approach is somewhat similar to the use of equivalent spheres, but is instead relating to an equivalent oblate. Calculations for  $\chi_{Oblate}$  for PRINT particles were performed by assuming dimensions of an oblate which completely encapsulated the PRINT particle dimensions. PRINT particle dimensions were determined through SEM measurements and  $\chi_{Oblate}$  were evaluated for two orientations of the encapsulating oblate using expressions by Loth.<sup>13</sup>

## Results and Discussion

### Particle fabrication

Particles were fabricated using the PRINT molding platform, yielding high fidelity particles. A total of 14 shaped particles were investigated in these studies; representative SEM micrographs of these shapes are shown in Figure 4. The most basic of these shapes was a cylinder and a two-dimensional (2-D) ellipsoid. Increasing in shape complexity, two overlaid ellipsoids comprised the Lorenz particle design. A series of pollen-mimic particles was inspired to replicate the highly dispersable properties of pollen spores. Figure 4A shows the cylinder, ellipsoid, Lorenz particles and the pollen-mimic series. To investigate the effect of fenestrations or macrosized pores, a series of three toroids of increasing diameter, as well as a hexagon with a circular cut-out dubbed “hexnut”, were fabricated. Finally, a “ball-and-stick” family of four shapes, referred to as a lollipop, v-boomerang, l-dumbbell and helicopter, was fabricated to explore effects of asymmetry. Figure 4B shows the fenestrated series and Figure 4C shows the ball-and-stick family. Measurements from these and similar micrographs produced particle dimensions. These are shown in Table 1, along with calculated values for  $D_{EV}$  and surface area. Length and width measurements listed represent the maximum dimension needed to enclose the particle in a solid oblate.

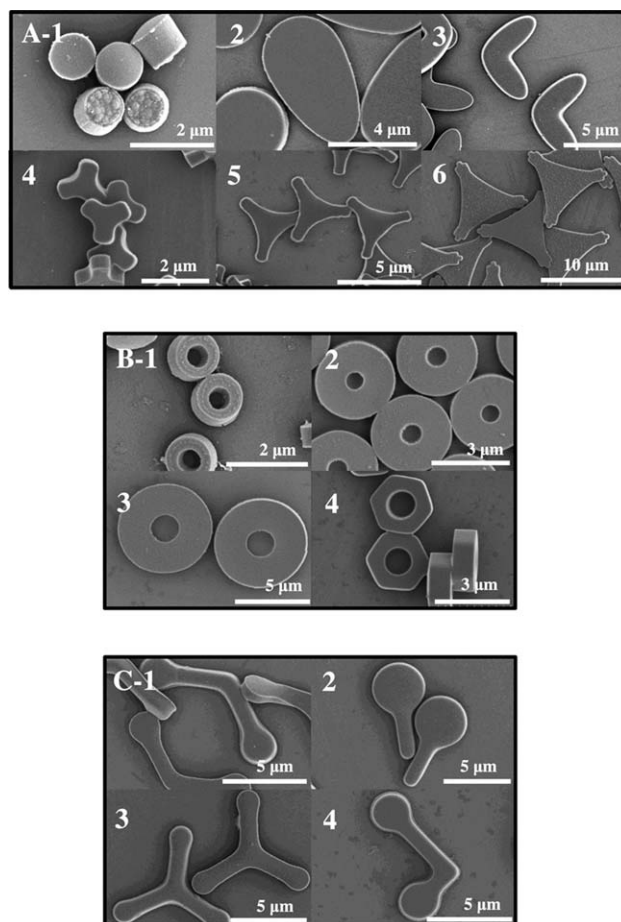


Figure 4. SEM micrographs of PRINT microparticles.

4A Curvature series and pollen-mimic series. A1) cylinder, A2) ellipsoid, A3) Lorenz, A4) small pollen-mimic, A5) medium pollen-mimic, A6) large pollen-mimic. 4B Fenestrated series. B1) small toroid, B2) medium toroid, B3) large toroid, B4) hexnut. 4C Ball-and-stick family. C1) v-boomerang, C2) lollipop, C3) helicopter, C4) l-dumbbell.

Bulk density measurements established the sample density to be  $1.17 \text{ g/cm}^3$ . This value was assumed for the density of PRINT particles.

### Aerosol characterization

Shaped PRINT particles were aerosolized with a CJN and sized with an APS. The CJN nebulizes a solution through a single jet, which collides with the chamber wall. This decreases the resultant liquid aerosol droplet size to  $2.5 \mu\text{m}$  with a GSD of 1.8, as reported by the manufacturer.<sup>39</sup> For our purposes, the liquid droplet features the most control final aerosol properties, as the methanol droplet completely evaporated to liberate particles. To confirm this, a simple calculation was performed to determine the rate of evaporation of a pure methanol droplet in dry conditions; the calculated lifetime of the droplet was  $\sim 3 \text{ ms}$ .<sup>9</sup> The lengthy drying column and placement of controlled leaks in the tubing ensured favorable conditions for evaporation. By adding a dilute suspension of particles in the liquid reservoir of the CJN, single particles were encapsulated in the emitted liquid droplets, which resulted in the creation of a monodisperse aerosol upon methanol evaporation. A complete listing of APS results is shown in Table 1, with representative results

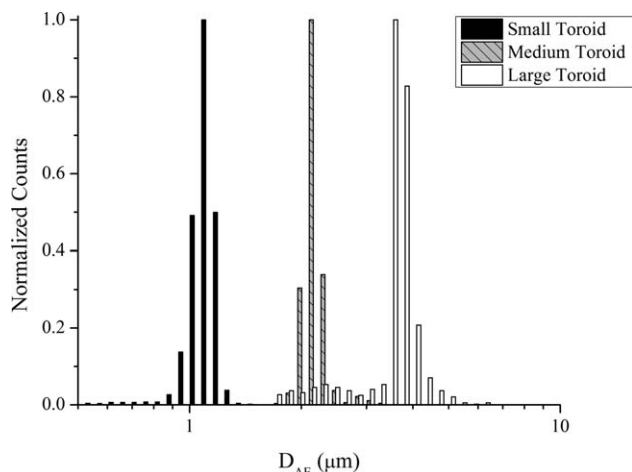
**Table 1. Measured and Tabulated Particle Characteristics**

Name	GEOMETRIC DIMENSIONS					AEROSOL PROPERTIES		
	Length ( $\mu\text{m}$ )	Width ( $\mu\text{m}$ )	Height ( $\mu\text{m}$ )	Surface Area ( $\mu\text{m}^2$ )	$D_{EV}$ ( $\mu\text{m}$ )	APS Sizing		Corrected $D_{AE}$ ( $\mu\text{m}$ )
						NMAD ( $\mu\text{m}$ )	GSD	
Cylinder	1.21	1.21	0.78	5.29	1.20	1.262	1.079	1.26
Ellipsoid	6.49	3.62	0.97	52.53	3.24	2.679	1.070	2.88
Lorenz	5.98	5.98	0.97	63.54	3.37	2.452	1.075	2.69
Small Pollen	1.45	1.45	0.60	4.69	1.02	1.120	1.121	1.11
Medium Pollen	3.39	3.39	0.35	17.51	1.63	1.215	1.201	1.27
Large Pollen	10.90	10.90	0.43	117.2	3.48	2.163	1.109	2.22
Small Toroid	1.26	1.26	0.74	6.25	1.13	1.111	1.100	1.12
Medium Toroid	3.36	0.36	0.87	28.09	2.41	2.088	1.066	2.19
Large Toroid	6.36	6.37	1.93	108.07	4.73	3.529	1.071	3.98
Hexnut	2.79	2.79	0.95	15.01	1.88	1.636	1.089	1.70
Lollipop	7.16	3.91	0.95	48.91	3.04	2.590	1.076	2.75
V-Boomerang	10.05	3.62	0.95	48.25	2.85	2.073	1.103	2.24
L-Dumbbell	6.19	4.05	0.88	41.16	2.71	2.184	1.073	2.33
Helicopter	6.11	6.11	0.88	47.57	2.74	1.978	1.103	2.14

Physical dimensions (length, width and height) for each geometry obtained through SEM measurements, with calculated values for surface area and  $D_{EV}$ . Aerosol properties are also shown, with APS sizing results for particles dispersed from a CJN and corrected  $D_{AE}$  corrected using the APS model.

for three toroid particles plotted in Figure 5. For all shaped particles tested, aerosol samples were highly monodisperse, yielding narrow distributions. As demonstrated in Figure 5, slight variations in geometry resulted in finely tuned NMADs. Reported GSDs for all shapes were less than 1.20, indicating that all samples displayed monodisperse characteristics in aerosol form. Even highly nonspherical particles, such as the large pollen-mimic, resulted in a GSD of less than 1.22. This characterization demonstrated that under proper dispersal conditions, PRINT particles can result in truly monodisperse aerosols.

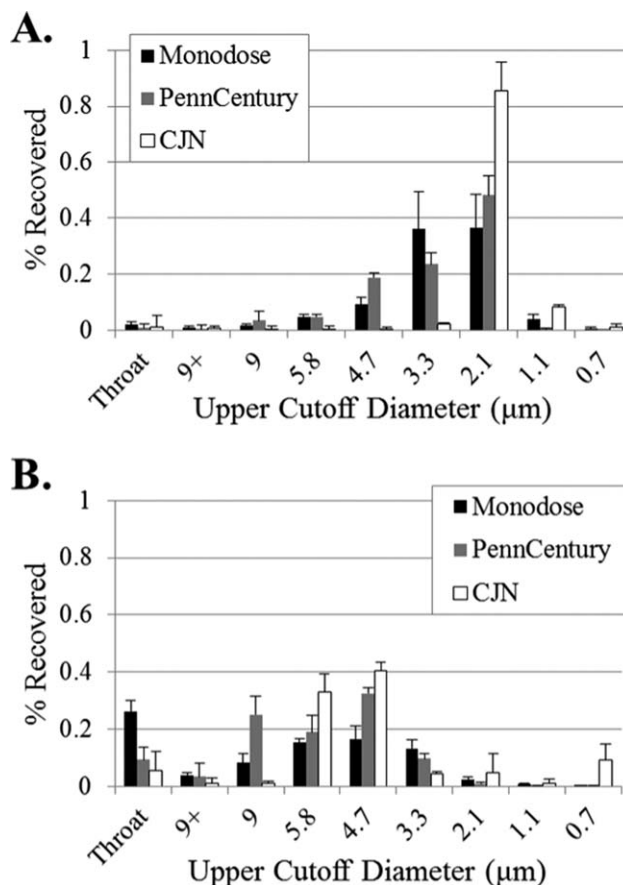
Additionally, two PRINT particle types were aerosolized using three aerosol devices and sized with an ACI. ACI measurements are the gold standard for obtaining aerodynamic diameters, especially in the pharmaceutical industry, as results can directly correlate to lung deposition.<sup>40</sup> Figure 6A and B show ACI mass distributions of small and large pollen-mimic aerosol samples, with MMAD and GSD reported in Table 2. Differences in dispersion device greatly impacted the quality of the aerosol sample; these devices will be discussed further following shape factor results.



**Figure 5. APS number results for fenestrated toroid series.**

### Shape factor determination with APS model

The APS numerical approach was utilized to determine  $\chi_{APS}$  and correct  $D_{AE}$  from APS measurements. Corrected  $D_{AE}$  are shown in Table 1 for each geometry. In Figure 7, measured values of  $D_{APS}$  are plotted against corrected  $D_{AE}$ , emphasizing the importance of correcting APS values for nonspherical aerosols. Also included in Figure 7 are two



**Figure 6. ACI distributions plotted as % deposition on each stage for (A) small pollen-mimic, and (B) large pollen-mimic powder samples.**



**Table 2. ACI Results for Small and Large Pollen-Mimic Powder Samples, Dispersed from Three Different Device Types**

Shape	$D_{EV}$	$D_{AE}$ Predicted	CJN		PennCentury		Monodose	
			MMAD	GSD	MMAD	GSD	MMAD	GSD
Small Pollen	1.92	1.11	1.73	1.18	2.45	1.79	2.29	1.49
Large Pollen	3.48	2.22	4.35	1.23	4.72	1.32	4.34	1.32

reference curves predicted by this model: the relation of  $D_{APS}$  with  $D_{AE}$  for (1) a sphere, which, by APS calibration has a slope of 1, and (2) a nonspherical particle with  $\chi$  of 2. These curves were generated using the APS model over a range of particle sizes. The deviation between  $D_{AE}$  and  $D_{APS}$  increased as the particle volume increased, agreeing with previous results.<sup>19,32–34</sup> Nonspherical PRINT particles fall within a range of the two reference curves, illustrating the difference between the APS measurement and the corrected  $D_{AE}$ .

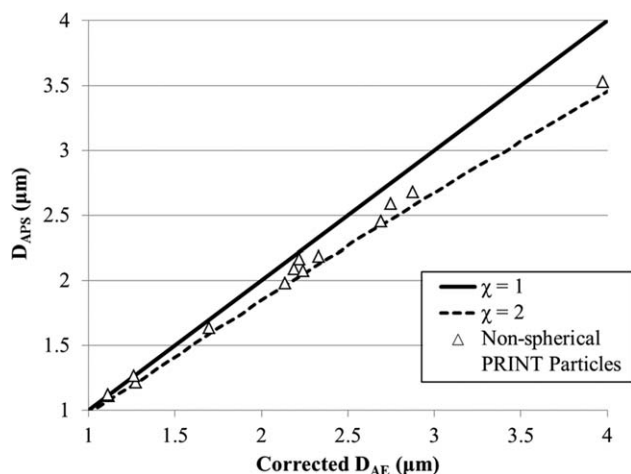
This approach uniquely utilizes APS measurements to determine shape factors for a particle of known volume. Values for  $\chi_{APS}$  ranged from slightly over one, to a maximum of 2.88 for the large pollen-mimic particles;  $\chi_{APS}$  for all shapes are reported in Table 3. The smallest deviation between  $D_{APS}$  and  $D_{AE}$  was observed for the cylinder particle, while the smallest reported shape factor was predicted for the small pollen-mimic. The size series of toroids and pollen-mimic particles exhibited increasing  $\chi_{APS}$  values with increasing particle diameter. Here, increase in overall volume emphasizes drag differences due to shape. The fenestrated design feature, such as those of the toroid series, resulted in increased particle  $\chi_{APS}$  as compared to a cylinder. However, intentional mass asymmetries from the placement of unequal arm lengths, such as the lollipop and l-dumbbell, did not result in increased  $\chi_{APS}$ . More symmetric analogs, such as the helicopter and v-boomerang, were determined to have a larger  $\chi_{APS}$ .

An increased shape factor offers unique opportunities specifically for respiratory drug delivery. A large shape factor will reduce the  $D_{AE}$  while maintaining a certain volume. Larger volume particles can deliver an increased therapeutic payload, leading to increased efficacy and dose sparing, while particles of a smaller  $D_{AE}$  can penetrate deeper into the lung parenchyma at higher efficiencies.<sup>11</sup> This has been

established using spray dried, large porous particles where the particle density modulates the  $D_{AE}$ .<sup>41</sup> Here, particle shape is instead implemented to modulate  $D_{AE}$  through enhancement of particle shape factor. Controlled geometry has other potential implications for respiratory drug delivery, as the interaction between the particle and the local lung environment will be heavily dependent on particle geometry. Particles with large shape factors will be capable of delivering a higher therapeutic deeper into the lung as compared to a spherical particle. From these results, flat, symmetric designs and fenestrated features contributed to increased shape factor; future designs combining these two qualities may yield even more sizeable shape factor predictions.

To validate these findings for shape factor on this set of particle geometries, comparisons can be made to the literature. There is a limited set of accepted shape factors for specific particles; these shape factors have generally been established for regular geometries and dust particles using sedimentation experiments.<sup>9,14–17</sup> From this limited collection, some correlations can be made to APS numerical model results. In the literature, the dynamic shape factor for a cylinder with an aspect ratio of 2 is reported to range from 1.01 (vertical orientation) to 1.14 (horizontal), with the averaged orientation 1.09. This averaged value matches exactly with the shape factor reported by the APS model. Further comparisons to shape factors reported in the literature can be made between talc powder and the symmetric, plate-like particles, such as the large pollen-mimic and helicopter geometries. Talc particles are thin symmetric plates with a high aspect ratio and large-surface area, resulting in reported experimental shape factors as high as 2.3. Additionally, a plate-like geometry has been theorized to yield shape factors approaching 3 for certain orientations.<sup>14</sup> These values correlate well with the large shape factor value of 2.88 for the large pollen-mimic geometry, which closely resembles a flat plate.

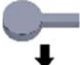

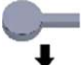
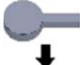

In many cases, direct comparisons to existing shape factor values cannot be performed due to the lack of existing data; alternative approximations must be taken to determine shape factors of a given geometry. To further validate the  $\chi_{APS}$  approach, shape factors for the novel shapes presented here were compared to three existing approaches (1) use of a sedimentation tank ( $\chi_{Sed}$ ), (2) calculation of shape factor using projected and surface area relations ( $\chi_{PSA}$ ), and (3) calculation of shape factor by approximating geometries of PRINT aerosols to an oblate ( $\chi_{Oblate}$ ). Results from the three approaches are compared to those of the APS model in Table 3. As is readily apparent from Table 3, these four approaches yield variable results for shape factors of nonspherical PRINT particles. Shape factors determined through the sedimentation tank and oblate approximation should reflect the maximum (Exp-H, Oblate-H) and minimum (Exp-V, Oblate-V) values for shape factors. Generally, the sedimentation tank is considered the gold standard as actual geometries are considered. APS model shape factors from a dynamic flow were anticipated to fall somewhere between



**Figure 7. Relation between experimentally measured  $D_{APS}$  values plotted against corrected  $D_{AE}$ .**



**Table 3. Shape Factor Results Determined from APS method, Compared to Results Determined from other Literature Methods: the PSA Method, Oblate Approximations, and Tank Sedimentation**

Shape	$\chi_{APS}$	$\chi_{Sedimentation}$ Exp-H	$\chi_{Sedimentation}$ Exp-V	$\chi_{PSA}$	$\chi_{Oblate-H}$	$\chi_{Oblate-V}$
						
Orientation	Averaged					
Cylinder	1.09	-	-	1.06	1.08	1.00
Ellipsoid	1.48	1.31	1.00	1.34	1.61	1.20
Lorenz	1.82	1.31	1.16	1.40	1.57	1.18
Small Pollen	1.03	-	-	1.15	1.20	1.01
Medium Pollen	1.91	-	-	1.55	1.82	1.31
Large Pollen	2.88	1.60	1.21	1.94	2.49	1.71
Small Toroid	1.22	-	-	1.17	1.10	1.00
Medium Toroid	1.44	1.05	1.00	1.28	1.36	1.08
Large Toroid	1.69	1.44	1.21	1.25	1.30	1.05
Hexnut	1.46	-	-	1.16	1.26	1.04
Lollipop	1.43	-	-	1.35	1.68	1.23
V-Boomerang	1.87	1.70	1.52	1.39	1.87	1.34
L-Dumbbell	1.57	1.52	1.23	1.37	1.64	1.21
Helicopter	1.91	2.01	1.69	1.43	1.63	1.21

these two extremes. As anticipated,  $\chi_{APS}$  were larger than the values for all  $\chi_{Sed}$  and  $\chi_{Oblate}$  in the vertical drag Exp-V/Oblate-V orientations; however,  $\chi_{APS}$  was also generally larger than those from horizontal Exp-H/Oblate-H orientations. Similarly,  $\chi_{APS}$  values were also generally larger in magnitude than  $\chi_{PSA}$ . The largest disagreement between  $\chi_{APS}$  and the three other approaches was always observed for the large pollen-mimic geometry, with the fenestrated particles (toroids and hexnut) and the Lorenz particles also consistently larger than the three literature predictions. However, this model did agree very well with simpler particle geometries. This agreement was especially true for cylindrical shaped particles, the most spherical shape tested, in which  $\chi_{PSA}$  and  $\chi_{Oblate}$  fell within 3% of  $\chi_{APS}$ .

The slight overestimation of the APS model might stem from a few sources. It is worthwhile to consider limitations of the mathematical expressions used for the model; the expression for sphericity in Eq. 6 has only been extended for shape factors ranging from 1 to 1.5, a range which is often exceeded with these highly nonspherical particles. Adding further complications, the particles tested here likely exhibited tumbling and rotational properties by design, which implies behaviors not represented in a single-shape factor. Rotation of particles, especially nonspherical ones, tremendously influences particle aerodynamic properties and their behavior under flow.<sup>10</sup> Furthermore, dynamic shape factors do not take into account particle orientation in the flow stream. These are two major considerations which are not included in any shape factor classification. Indeed, the standard approaches for determining particle shape factor used as validation here also fail to capture dynamic behavior. Values of shape factor determined by each of the three commonly implemented methodologies also do not account for rotation of particles in flow. For example, the simplification of particles to an oblate approximation based on the maximum length, width, and height of the particle removes any possible effect of mass asymmetry and will fail to capture realistic particle motion of the true geometry. Additionally, these three literature approaches all relate to macroscale models, rather than true aerosols;  $\chi_{PSA}$  and  $\chi_{Oblate}$  were derived to fit  $\chi_{Sed}$  literature results. Poor agreement for shapes which are

increasingly nonspherical, such as the pollen-mimic and toroids that have geometrical design features such as fenestrations and high aspect ratio, contributed to the hypothesis that these asymmetric PRINT particles were exhibiting characteristics which cannot be well represented with current approaches of shape factor.

Despite these discrepancies, characterization of shape factor still holds value as a characterization parameter for nonspherical PRINT aerosols. The rapid conversion to aerodynamic diameter and the ability to harness knowledge of particle deposition, especially for respiratory delivery, makes shape factor a powerful tool. Indeed, knowledge of particle geometries which are no longer well described by shape factors will aid in additional research focuses and design parameters. Future studies into particle dynamics of unique geometries will be required to adequately model the individual features of each design. Computational approaches using a Lagrangian framework and solid body dynamics can provide insight to the complicated relations between particle geometry and surrounding flow; an accurate model of such a system would consider fluid-particle coupling and the role of torque and lift on a single particle.<sup>10,42</sup> This more complex approach would account for these potentially considerable influences and support the hypothesis that nonspherical particles presented here are exhibiting interesting dynamic behavior. Such a model would also provide guidelines of particle geometries where a reduction to a single shape factor value would be no longer useful. Despite the limitations of using a dynamic shape factor, the rapid screening approach presented here yielded reasonable and descriptive shape factors for these novel shapes and likely captured more of the dynamic behavior of a true aerosol under flow than standard approaches used for comparison. Fitting to experimental APS results is also preferable to the tedious experiments involved with a sedimentation tank.

Overall, the model presented here for determining shape factors by correcting APS results agreed reasonably with existing approaches, with generally only slight overestimation of dynamic shape factors for most geometries. The agreement between  $\chi_{APS}$  and literature values,  $\chi_{PSA}$ , and  $\chi_{Oblate}$  for the cylinder validate the APS numerical approach

and allowed for classification of these nonspherical PRINT particles.

**Application of Determined Shape Factors.** Determining shape factors for nonspherical particles allowed for the prediction of  $D_{AE}$  for a given particle geometry. This is valuable when evaluating more realistic powder samples, such as the small and large pollen-mimic samples aerosolized in Figure 6 and Table 2. Dispersing dry powders and overcoming aggregation for particles of this size range remains a challenge for formulation scientists; electrostatics and van der Waals forces play a significant role in powder agglomeration. To assess which device more adequately dispersed dry powder samples, sizing results of these true dry powder aerosols were compared to the theoretical prediction of the same shaped monodisperse particle. In combination with ACI sizing, the various aerosol dispersion devices resulted in aerosol populations with larger MMADs than the predicted monodisperse aerosol. This can in part be attributed to the low resolution of the ACI stage cutoff values, highlighting discrepancies between aerosol sizing techniques. From previous APS sizing, the aerosol resulting from the CJN was assumed to be monodisperse; indeed, the large and small pollen-mimic aerosols dispersed from the CJN had the smallest MMADs of the three devices and GSDs of about 1.2. Interestingly, the monodisperse large pollen-mimic aerosol deposited evenly on stages 3 and 4, which contributes to the increased MMAD. Compared to these monodisperse aerosols, samples dispersed from either the Monodose inhaler or the PennCentury exhibited increased signs of aggregation. Both devices resulted in larger MMADs than predicted for the two particle geometries; of the three, the MMAD increase for aerosol samples created by the PennCentury was the most substantial. However, deposition on earlier stages and the ACI throat was indicative of larger agglomerates present in aerosols from both devices. These trends were apparent in the distribution presented in Figure 6 and supported by the elevated MMAD, but were not necessarily apparent through comparison of each sample's GSD, the typical indicator of aggregation. Comparison to the predicted monodisperse  $D_{AE}$  for each particle geometry allowed for more detailed evaluation of these devices by providing a theoretical reference.

Defining a deviation from the theoretical monodisperse particle lends qualitative insight as to the nature of the aerosols produced. This will be especially useful in comparing dispersion of nonspherical aerosols and predicting deposition. Future compositions of the same physical particle geometry can be evaluated against the theoretical monodisperse value. Establishing baseline features of individual particle dynamics, including properties such as  $D_{AE}$ , is critical to probing more complicated processes of realistic samples. The ACI results of dry powder PRINT samples illustrated that agglomerates were still present, but also that a large fraction of both samples behaved as individual particles, indicated by deposition on the same stage as the monodispersed aerosol. Establishing the theoretical monodisperse  $D_{AE}$  allows for differentiation of the dose fraction comprised of individual particles. Deagglomeration under dynamic conditions is representative of typical respiratory doses; larger agglomerates will impact in the throat and liberated individual particles will deposit in the lung as predicted by  $D_{AE}$ . Typical ACI sizing which does not compare to a monodisperse sample artificially inflates the MMAD and fails to identify the fraction of the dose which

deposits in the region of interest. While initial dispersion from the inhaler device is important, deposition in the target lung region will be achieved by individual particles. Following deposition, the rate of mucociliary clearance, cellular interactions, macrophage uptake, and drug release kinetics will also be a function of individual particle properties. As such, the physical, chemical, and aerodynamic characterization of individual particles holds tremendous value. In this context, our method for determining shape factors of nonspherical novel geometries provides a rapid approach to better characterize well-defined aerosol particles. This methodology further can be applied to any aerosol of controlled particle geometry, as only  $D_{EV}$  of a uniform population is required.

## Conclusion

The work presented here introduces a class of novel shaped aerosols; using PRINT technology, truly monodisperse shaped aerosols were generated. From this complete control over particle uniformity resulting in a known particle size, a correction to APS sizing techniques was employed to characterize particle shape factors for this series of particles. This approach yielded shape factors in reasonable agreement with the limited approaches present in the literature. Limitations of using particle shape factor as a descriptive parameter were also discussed, which will be critical in further design approaches to nonspherical aerosols. As more complex geometries of aerosol particles are explored, additional characterization parameters will be required to accurately represent dynamic behavior. However, modifying the APS use as described enables a rapid classification technique for determining useful and translatable features of shaped particles, which can be implemented for respiratory delivery indications. Classifying shaped particles with a dynamic shape factor allows for a quick calculation of a theoretical  $D_{AE}$ , deviation from which lends insight to sources of particle aggregation when aerosolized from standard inhalers.

Implementing designed nonspherical particles for respiratory drug delivery offers unique aerodynamic properties; increasing shape factor will lead to decreased  $D_{AE}$  and deeper lung deposition. Improving our analysis of this set of nonspherical PRINT aerosols enhances their applicability to address increasingly complicated questions in aerosol and respiratory topics. Controlling particle shape of a dry powder formulation allows for the opportunity to create monodisperse shaped aerosols with potential to systematically optimize the effect of shape on the many stages of drug delivery. Ideally, *a priori* knowledge of particle behaviors of a given formulation and dispersion method could be used to design a controlled therapeutic response. Future directions for our work include addressing how particle shape can mitigate powder agglomeration and aid in appropriate cellular delivery. We also intend to explore advanced modeling approaches to better describe the role of geometry in particle aerodynamics in the lung. Overall, this approach for predicting and characterizing particle shape factor on calibration quality particles extends our knowledge of particle interactions as aerosols and may ultimately be used to better guide the design and engineering of particles for pulmonary delivery.

## Acknowledgments

We thank Joe Pedit, Maryanne Boundy and David Leith for sharing their APS and for many helpful discussions of

aerosol sizing, Steve Emanuel for fabrication of macroscale model parts, the CHANL facility at UNC for use of the SEM, Stuart Dunn and John Fain, Sorin Mitran, and Katherine Phillips for useful discussions regarding PRINT particle fabrication, rigid body dynamics, and MATLAB, respectively, and for and Liquidia Technologies for providing molds. This work was supported by Liquidia Technologies and the National Institutes of Health Director's Pioneer Award (1DP1OD006432).

## Literature Cited

- Weers JG, Bell J, Chan HK, Cipolla D, Dunbar C, Hickey AJ, Smith IJ. Pulmonary formulations: what remains to be done? *J Aerosol Med Pulm Drug Deliv.* 2010;23(Suppl 2):S5–23.
- Daniher DI, Zhu J. Dry powder platform for pulmonary drug delivery. *Particuology.* 2008;6:225–238.
- Calvert G, Ghadiri M, Tweedie R. Aerodynamic dispersion of cohesive powders: A review of understanding and technology. *Adv Powder Technol.* 2009;20:4–16.
- Kleinstreuer C, Zhang Z, Donohue JF. Targeted drug-aerosol delivery in the human respiratory system. *Annu Rev Biomed Eng.* 2008;10:195–220.
- Hassan MS, Lau RW. Effect of particle shape on dry particle inhalation: study of flowability, aerosolization, and deposition properties. *AAPS PharmSciTech.* 2009;10:1252–1262.
- Louey MD, Oort MV, Hickey AJ. Aerosol dispersion of respirable particles in narrow size distributions using drug-alone and lactose-blend formulations. *Pharm Res.* 2004;21:1207–1213.
- Usmani OS, Biddiscombe MF, Barnes PJ. Regional lung deposition and bronchodilator response as a function of beta2-agonist particle size. *Am J Respir Crit Care Med.* 2005;172:1497–1504.
- Brand P, Meyer T, Sommerer K, Weber N, Scheuch G. Alveolar deposition of monodisperse aerosol particles in the lung of patients with chronic obstructive pulmonary disease. *Exp Lung Res.* 2002;28:39–54.
- Hinds WC. Aerosol Technology: Properties, Behaviour and Measurement of Airborne Particles. New York: Wiley-Interscience; 1999.
- Zastawny M, Mallouppas G, Zhao F, van Wachem B. Derivation of drag and lift force and torque coefficients for non-spherical particles in flows. *Int J Multiphase Flow.* 2012;39:227–239.
- Crowder TM, Rosati JA, Schroeter JD, Hickey AJ, Martonen TB. Fundamental effects of particle morphology on lung delivery: predictions of Stokes' law and the particular relevance to dry powder inhaler formulation and development. *Pharm Res.* 2002;19:239–245.
- Lippmann M. Size-selective health hazard sampling. In: *Air Sampling Instruments for Evaluation of Atmospheric Contaminants*. Cincinnati, OH: ACGIH; 1995.
- Loth E. Drag of non-spherical solid particles of regular and irregular shape. *Powder Technol.* 2008;182:342–353.
- Cheng Y-S, Yeh H-C, Allen MD. Dynamic shape factor of a plate-like particle. *Aerosol Sci Technol.* 1988;8:109–123.
- Johnson DL, Leith D, Reist PC. Drag on non-spherical, orthotropic, aerosol particles. *J Aerosol Sci.* 1987;18:87–97.
- Cheng Y-S. Drag forces on nonspherical aerosol particles. *Chem Eng Commun.* 1991;108:201–223.
- Davies CN. Particle-Fluid Interaction. *J Aerosol Sci.* 1979;10:477–513.
- Leith D. Drag on nonspherical objects. *Aerosol Sci Technol.* 1987;6:153–161.
- Brockmann JE, Rader DJ. APS Response to nonspherical particles and experimental determination of dynamic shape factor. *Aerosol Sci Technol.* 1990;13:162–172.
- Geiser M, Schurch S, Gehr P. Influence of surface chemistry and topography of particles on their immersion into the lung's surface-lining layer. *J Appl Physiol.* 2003;94:1793–1801.
- Champion JA, Mitragotri S. Shape induced inhibition of phagocytosis of polymer particles. *Pharm Res.* 2009;26:244–249.
- Gratton SE, Ropp PA, Pohlhaus PD, Luft JC, Madden VJ, Napier ME, DeSimone JM. The effect of particle design on cellular internalization pathways. *Proc Nat Acad Sci USA.* 2008;105:11613–11618.
- Patton JS, Byron PR. Inhaling medicines: delivering drugs to the body through the lungs. *Nat Rev Drug Discov.* 2007;6:67–74.
- Rolland JP, Maynor BW, Euliss LE, Exner AE, Denison GM, DeSimone JM. Direct fabrication and harvesting of monodisperse, shape-specific nanobiomaterials. *J Am Chem Soc.* 2005;127:10096–10100.
- Kelly JY, DeSimone JM. Shape-specific, monodisperse nanomolding of protein particles. *J Am Chem Soc.* 2008;130:5438–5439.
- Garcia A, Mack P, Williams S, Fromen C, Shen T, Tully J, Pillai J, Kuehl P, Napier M, Desimone JM, Maynor BW. Microfabricated engineered particle systems for respiratory drug delivery and other pharmaceutical applications. *J Drug Deliv.* 2012;2012:941243.
- Lee C-T, Leith D. Drag force on agglomerated spheres in creeping flow. *J Aerosol Sci.* 1989;20:503–513.
- Kasper G, Niida T, Yang M. Measurements of viscous drag on cylinders and chains of spheres with aspect ratios between 2 and 50. *J Aerosol Sci.* 1985;16:535–556.
- Baron PA. Calibration and use of the aerodynamic particle sizer (APS 3300). *Aerosol Sci Technol.* 1986;5:55–67.
- Wang H-C, John W. A simple iteration procedure to correct for the density effect in the aerodynamic particle sizer. *Aerosol Sci Technol.* 1989;10:501–505.
- Tsai C-J, Chen S-C, Huang C-H, Chen D-R. A universal calibration curve for the TSI aerodynamic particle sizer. *Aerosol Sci Technol.* 2004;38:467–474.
- Marshall IA, Mitchell JP, Griffiths WD. The behaviour of regular-shaped non-spherical particles in a TSA aerodynamic particle sizer. *J Aerosol Sci.* 1991;22:73–89.
- Cheng YS, Chen BT, Yeh HC. Behaviour of isometric nonspherical aerosol particles in the aerodynamic particle sizer. *J Aerosol Sci.* 1990;21:701–710.
- Cheng YS, Chen BT, Yeh HC, Marshall IA, Mitchell JP, Griffiths WD. Behavior of compact nonspherical particles in the TSI aerodynamic particle sizer model aps33b: ultra-stokesian drag forces. *Aerosol Sci Technol.* 1993;19:255–267.
- Rasband WS. Image J. In: *Health USNI*, ed. Bethesda, MD; 1997–2012.
- Density Determination of Solids. In: *Instruction Manual for Mettler-Toledo Density Kit*. Mettler-Toledo; 2002.
- Chapter 601-Physical tests and determinations: aerosols USP 26-NF 21. 2003:2105–2123.
- MATLAB. In: Natick, MA: The MathWorks, Inc.; 2003.
- BGI Incorporated. Collision Nebulizer Droplet Number Output. Available at: [http://www.bgiusa.com/agc/droplet\\_number\\_output.htm](http://www.bgiusa.com/agc/droplet_number_output.htm). Accessed: July 1, 2012.
- Thiel CG. Can in vitro particle size measurements be used to predict pulmonary deposition of aerosol from inhalers? *J Aerosol Med.* 1998;11:S43–S52.
- Edwards DA. Large porous particles for pulmonary drug delivery. *Science.* 1997;276:1868–1872.
- Tu J, Kiao I, Ahmadi G. *Computational Fluid and Particle Dynamics in the Human Respiratory System*. New York: Springer; 2013.

Manuscript received Nov. 3, 2012, and revision received May. 22, 2013.